Single-crystal infrared and Raman spectroscopic study of methylammonium and propylammonium tetrachloromanganate(II), (MAMC and PAMC)

1978 J. Phys. C: Solid State Phys. 11 617

(http://iopscience.iop.org/0022-3719/11/3/022)

J. Phys. C: Solid State Phys., Vol. 11, 1978. Printed in Great Britain. © 1978

Single-crystal infrared and Raman spectroscopic study of methylammonium and propylammonium tetrachloromanganate(II), (MAMC and PAMC)

D M Adams and D C Stevens
Department of Chemistry, University of Leicester, Leicester LE1 7RH, UK

Received 8 February 1977, in final form 28 September 1977

Abstract. Infrared reflectance spectra are reported for oriented single crystals of MAMC and PAMC with the electric vector parallel to the anionic sheets for temperatures from 50 to 295 K. Single-crystal Raman spectra were also obtained at similar temperatures. The main features of the spectra, particularly for the ambient temperature phases, are assigned with the aid of a factor group analysis. This phase for MAMC, although orthorhombic, behaves spectroscopically as pseudo-tetragonal, but PAMC is plainly orthorhombic. Modes above 260 cm^{-1} are attributed to cation internal modes, including torsions. The phase III (tetragonal) to phase IV (monoclinic) transition is distinguished in the Raman spectra by disappearance of an intense broad feature at about 35 cm^{-1}.

1. Introduction

The group of materials of the type $[C_nH_{2n+1}NH_3]_2[MCl_4]$, (M = Cr, Mn, Fe, Cu, Cd), have structures in which $[MCl_4^{2-}]_m$ layers are isolated from each other by interposed sheets of cations. Even for $n = 1$ (i.e. methyl) the separation is considerable and layers are sufficiently well isolated that they form excellent model systems in which magnetic phenomena in two dimensions may be studied. All these materials exhibit several phase changes associated with varying degrees of ordering of the hydrogen-bonding between cations and $[MCl_4^{2-}]_m$ layers. These structural transitions have recently excited much interest as shown by the neutron (Knorr *et al* 1974, Heger *et al* 1975, 1976) and x-ray (Chapuis *et al* 1975, 1976) diffraction, dielectric (Levstik *et al* 1976), optical birefringence (Knorr *et al* 1974), calorimetric (Arend *et al* 1973, Bocanegra *et al* 1975), NMR and NQR (Brinkmann *et al* 1976, Kind and Roos 1976, Seliger 1976, Blinc *et al* 1977), and vibrational spectroscopic (Lehner *et al* 1975, Stoelinga and Wyder 1976) data that have been reported, mostly within the last two years. In all but the lowest temperature (monoclinic) phases there is disorder associated with the cations. These systems are attractive spectroscopically in that much is already known about their structures and the types of disorder shown, and there are many members of the series. Moreover, a proper understanding of their lattice dynamical behaviour is important in elucidating the mechanisms of the phase changes.

We report the results of studies by single-crystal IR and Raman techniques on $[CH_3NH_3]_2MnCl_4$ (MAMC) and $[C_3H_7NH_3]_2MnCl_4$ (PAMC) for which some structural data are available. The full vibrational assignment is a matter of great complexity which will require extensive further work. What we report is the characterisation by

both IR and Raman spectroscopy of three of the phases of MAMC, and similar work on PAMC, together with a first-order assignment.

MAMC is known to undergo the phase transitions shown in table 1. The structures of the high-temperature tetragonal and the orthorhombic forms have been determined by neutron diffraction (Heger *et al* 1975), and an x-ray diffraction study has been made of the equivalent orthorhombic form of PAMC (Peterson and Willett 1972). The structures of all these forms, and those of the analogous iron and copper series, are based upon that of K_2NiF_4. This consists of infinite sheets of metal atoms in approximate octahedral coordination joined by sharing four common vertices in a plane. The relationship of this structure to that of perovskite is obtained by noting that Mn occupies B-sites, whilst the A sites in the cavities between the octahedra are filled by cations (Arend *et al* 1973).

Table 1. Phase transitions in $(CH_3NH_3)_2\ MnCl_4$.†

Phase	Structure	Transition temperature (K)	Transition type
I	Tetragonal, *I4/mmm* (D_{4h}^{17})		
		393·8	second order
II	Orthorhombic, *Abma* (D_{2h}^{18})		(order–disorder)
		257	first order
III	Tetragonal, *P4/ncm* (D_{4h}^{16})		
		94	first order
IV	Monoclinic		
		45	second order
V	Monoclinic (antiferromagnetic)		

† Heger *et al* (1975), Arend *et al* (1973).

2. Theory

The room temperature orthorhombic phase of MAMC crystallises with the symmetry *Cmca* (D_{2h}^{18}) with a bimolecular primitive cell. Heger *et al* (1975) used the non-standard setting *Abma*. In comparing spectra obtained by our two groups it is necessary to bear in mind the equivalences:

Cmca	*c*	*a*	*b*
Abma	*a*(7·276)	*b*(7·215)	*c*(19·41)

where unit cell parameters are given in parentheses. The anionic sheets lie in *ac* planes in *Cmca*. The room temperature form of PAMC, has an equivalent structure (Peterson and Willett 1972) to that of phase II of MAMC with $a = 7{\cdot}29$, $b = 25{\cdot}94$, and $c = 7{\cdot}51$ Å.

In understanding the construction of the spectra it is helpful to consider first the parent structure type, K_2NiF_4. This contains a single anion layer of symmetry isomorphous with D_{4h}, with a unimolecular repeat. The factor group analysis (FGA) is given in table 2(*a*). The $3n - 3 = 12$ internal modes of the sheet span the representation (1).

$$A_{1g} + E_g + 2A_{2u} + B_{2u} + 3E_u. \tag{1}$$

Such a sheet therefore yields two Raman and five IR-active bands (B_{2u} is inactive). In particular the modes principally due to M–halogen bond stretching are $A_{1g} + A_{2u}$,

Table 2. Factor group analyses for orthorhombic $(CH_3NH_3)_2\ MnCl_4$ and K_2NiF_4.
(*a*) $(CH_3NH_3)_2\ MnCl_4$ (*Cmca*, $z = 4$)

D_{2h}^{18}	A_g	B_{1g}	B_{2g}	B_{3g}	A_u	B_{1u}	B_{2u}	B_{3u}
Mn (2*a*)†					1	2	2	1
Cl_b (4*e*)	1	2	1	2	1	2	1	2
Cl_t (4*f*)	2	1	1	2	1	2	2	1
N_C	2	1	1	2	1	2	2	1
N_T	5	4	3	6	4	8	7	5
T_A						1	1	1
N_S	3	3	2	4	3	5	4	3
T	2	1	1	2	1	2	2	1
R	1	2	2	1	2	1	1	2
τ		1	1		1			1
IR						z	y	x
Raman	x^2, y^2, z^2	xy	xz	yz				

† Wyckoff sites in parentheses.
N_C = N atoms of cations; N_T total number of modes of unit cell, taking $CH_3NH_3^+$ as monatomic and is sum of preceding rows; T_A acoustic modes; N_S = internal modes of sheet; T translatory modes of $CH_3NH_3^+$; R rotatory modes of $CH_3NH_3^+$ (not included in sum, N_T); τ torsions of $CH_3NH_3^+$ (not included in N_T).

(*b*) K_2NiF_4 (*I4/mmm*, $z = 2$)

	A_{1g}	A_{2g}	B_{1g}	B_{2g}	E_g	A_{1u}	A_{2u}	B_{1u}	B_{2u}	E_u
N_T	2				2		4		1	5
T_A							1			1
N_S	1				1		2		1	3
$T(K^+)$	1				1		1			1
IR							z			(x, y)
Raman	$x^2 + y^2$ z^2				(xz, yz)					

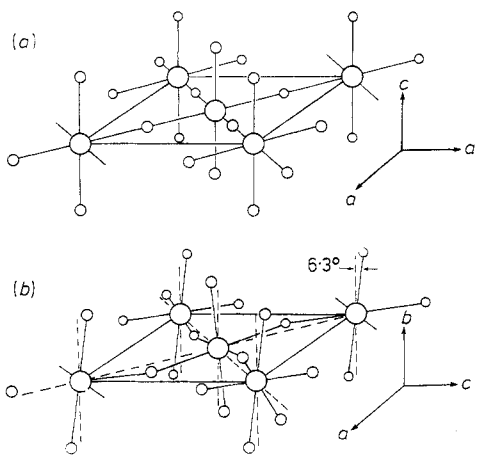

Figure 1. (*a*) The high-symmetry sheet structure of K_2NiF_4 and, (*b*) the distorted form present in MAMC phase II.

M–halogen (terminal); and E_u, M–halogen (bridge). All these sheet modes have been located in SnF_4, (Beattie *et al* 1971), for example, at 621(A_{1g}), 230(E_g); 730, 436 (A_{2u}); 472, 262, 245 (E_u) cm^{-1}; and in K_2NiF_4 at 385(A_{1g}), 133(E_g) cm^{-1} (Lehmann and Weber 1973).

In the room temperature phase of MAMC the metal atoms retain the approximately octahedral coordination of the SnF_4 sheet type but are tilted 6·3° out of plane in the manner illustrated in figure 1 to give a wavy sheet. Each metal atom has D_{4h} local symmetry but is on a site of C_{2h} ($C_2(x)$) symmetry. Two ($MnCl_4$) units are now required to define the repeat unit of the sheet which therefore has $3n' - 3 = 27$ internal modes. An FGA of MAMC is given in table 2(*a*); row N_S shows the representation spanned by the 27 sheet modes. An unusual situation arises in this FGA. There are two wavy sheets per unit cell, *Cmca*, which has $z = 4$. In the corresponding primitive cell (which must be used for the vibrational analysis) there are only two formula units, one from each sheet; the Mn atoms are at (0 0 0), (0 $\frac{1}{2}$ $\frac{1}{2}$). However, physically the vibrational interactions between sheets are effectively zero (although there is magnetic interaction below 44·5 K) (Heger *et al* 1973) but, if the spectra are to be considered on the basis of the behaviour of an isolated quasi two-dimensional sheet, a bimolecular repeat must be chosen for the sheet. When these sheets are stacked in *Cmca* the symmetry relations between them reduce the vibrational requirement to one formula unit per sheet in the three-dimensional primitive cell.

Some insight into the meaning of the rather complex vector N_S may be had by considering the contributions to it from normal modes which are chiefly due to Mn–Cl stretching. These will be the highest of the sheet modes. Established assignments for other chloro-complexes of manganese indicate that in MAMC ν(Mn–Cl) modes will not be higher than 260 cm^{-1}. Thus: $[(CH_3)_4N][MnCl_3]$ (chain structure, metal octahedrally coordinated to chlorines) has its highest Raman and IR-active bands at 256, 224 cm^{-1} respectively (Adams and Smardzewski 1971). For $CsMnCl_3.2H_2O$ these are at 213 and 256 cm^{-1} respectively (Adams and Newton 1971) and the coordination sphere consists of two water molecules, two terminal chlorines and two bridging chlorines. $[(C_2H_5)_3NH]_2$ $[MnCl_4]$ contains tetrahedral anions and is therefore expected to have higher frequency ν(Mn–Cl) modes than in the above compounds. It has $\nu_1(A_1)$ 256, $\nu_3(T_2)$ 278 cm^{-1} (Edwards *et al* 1968). $\nu(Mn^{II}–Cl)$ frequencies are among the lowest shown by compounds of the 3d-metals due to the lack of ligand field stabilisation energy.

In the SnF_4 type sheet at each metal atom the two Cl_t (t = terminal, b = bridge) atoms contribute six modes. The two stretching modes are A_{1g}, A_{2u}. In the wavy sheet structure of MAMC two such units couple via the site group as shown:

$$\begin{array}{lll} D_{4h} \rightarrow C_{2h}(C_2'') \overset{\times 2}{\rightarrow} D_{2h}^{18}(C_2(x)) & & \\ A_{1g} \quad A_g \quad\quad A_g + B_{3g} & & \\ A_{2u} \quad B_u \quad\quad B_{1u} + B_{2u} & & \end{array}$$

The same result follows directly from the vector of row 4F of *Cmca* (the Wyckoff sites of the Cl_t atoms) in table 3 of Adams and Newton (1970). $\nu(Mn–Cl_b)$ may be obtained similarly, namely, $A_u + B_{1u} + B_{2u} + B_{3u}$, but these bridge frequencies will be considerably lower than those of $\nu(Mn–Cl_t)$ if the pattern of SnF_4 is followed.

We now consider modes due to cations. $CH_3NH_3^+$ has no internal modes below 350 cm^{-1} apart from the torsion. Although the cation sheets are isolated from each other it is reasonable to suppose that their translatory modes may couple weakly across

the wavy sheets via low-frequency modes of the latter. This is described formally by row T of the FGA which gives the representation spanned by the three translatory motions of the four cations in the primitive cell (which contains four cations whether we take the primitive cell of the isolated sheet and its associated cations, or the x-ray cell). By comparison with simple salts such as $[Me_4N]_2[PtCl_6]$ and $[NH_4]_2[PtCl_4]$, it is expected that none of the translatory and rotatory lattice modes of $CH_3NH_3^+$ will be higher than about 120 cm^{-1}.

The representation of the cation internal torsional modes, τ, may be found by correlating from the ion group via its crystal site (4*f*).Thus:

$$\begin{array}{lll} C_{3v} \rightarrow C_s(\sigma(yz)) \overset{\times 4}{\rightarrow} D_{2h}^{18} & & \\ A_2(R_z) \quad A'' \qquad B_{1g} + B_{2g} + A_u + B_{3u} & & \end{array}$$

In C_{3v} this mode is neither IR nor Raman-active: its principal means of gaining activity is via the site field. This is apparently inadequate to cause it to develop significant IR intensity in the crystal but some Raman features are attributed to this origin, see below.

The above considerations show that (neglecting cation internal torsions) the total numbers of normal modes expected in each species are as shown in (2).

$$6A_g + 6B_{1g} + 5B_{2g} + 7B_{3g} + 6A_u + 8B_{1u} + 7B_{2u} + 6B_{3u}. \qquad (2)$$

Of these, $\nu(Mn\text{–}Cl_t)$ accounts for $A_g + B_{3g} + B_{1u} + B_{2u}$ and $\nu(Mn\text{–}Cl_b)$ for $A_u + B_{1u} + B_{2u} + B_{3u}$. The g-modes are all Raman-active and the B_{nu} modes are all IR-active.

Below 257 K a transition takes place to a tetragonal phase. The structure has not been reported in detail but the space group is $P4_2/ncm$ (D_{4h}^{16}) (Heger *et al* 1975). In this group none of the Wyckoff sites occur in sets of less than four: it follows that the primitive cell is tetramolecular and that it has doubled during the phase transition. The structure of the sheets is maintained if we place Mn on sites 4*d*(2/*m*), (000, $\frac{1}{2}$ 0 $\frac{1}{2}$, 0 $\frac{1}{2}$ $\frac{1}{2}$, $\frac{1}{2}$ $\frac{1}{2}$ 0); Cl_t on 8*i*(*m*), Cl_b on 8*g*(C_2), and the captions on 8*g*. In this structure there are two sheets per cell, each with a bimolecular repeat but, since the sheets are still physically isolated the spectrum must still be interpreted on the basis of the repeat unit of one sheet: this we do not know. If it has risen to four the coupling scheme within the sheet will be more complex but will still give an appearance of simplicity because degeneracies arise in a tetragonal group and the selection rules are more restrictive than in D_{2h}^{18}. In summary, there is unlikely to be much spectral change in the region about 150 to 250 cm^{-1} due to this phase transition, but minor changes may occur at lower frequencies in the lattice mode region.

There is no information on the structure of the monoclinic phase IV, which represents yet another way of accommodating the hydrogen-bonding requirements of the cations. However, a substantial increase in spectral complexity is to be expected on entering this phase from phase III. This follows because the somewhat restrictive IR and Raman activities of the higher-symmetry phases are relaxed to the extent that everything becomes either IR—or Raman-active and all degeneracies are lifted. These effects will be enhanced by band sharpening due to progressive removal of hot bands and second-order features from the spectra as the temperature is lowered.

3. Experimental details

The crystals were a gift from Dr L Dubicki of Monash University and were in the form of thin platelets about 1 to 2 mm thick and several mm side. The axial directions were checked by optical examination.

Table 3. IR frequencies (cm^{-1}) (ϵ'' maxima).

a PAMC	$E \| a$				$E \| c$			
Temperature (K)	50	100	190	295	50	100	190	295
	285	283	282	280	212	202	193	192
	272	267	273	257	187			
	247		222		174			
	206	192			159	159		
	175	172	167		143			
	159				133	131	121	120
	147	148	143	141	113			
	130	127	122	120	104	103	101	
	103	102	102	191	93	93	90	92
	92	90	87	85	66	67		
	69	70	73	68		46		
	59	57						
b MAMC								
		235			234	235		
	228	225	228	225	224	224	228	225
	201							
	182							
	162				162			
	147	158	150	141		157	147	142
	127	120			123	123		
	110	109	109	110	111	109	107	110
	100	100			99	100		
	88	92	93			92	93	
	71	72	73		70	70	75	
	63							

Table 4. Raman wavenumbers (cm^{-1}) for PAMC.

(*a*) Randomly oriented crystal, 100 K		
98 ± 1	192 ± 3	284 ± 5
121 ± 2	204 ± 3	
(*b*) Oriented single crystal, 100 K (see figure 3)		
c(*bc*)*b*	*c*(*aa*)*b*	
38 ± 5	37 ± 4	
74 ± 4	50 ± 5	
84 ± 4		
99 ± 1	99 ± 1	
120 ± 2	120 ± 2	
143 ± 3	136 ± 4	
~190–210	region of continuous	
240 ± 4	scatter with maxima about	
266 ± 5	190, 207, 275, and 290	
282 ± 5		

Table 5. Raman wavenumbers (cm^{-1}) for MAMC in phases III and IV†

a(*cc*)*b*		*a*(*ba*)*b*		*a*(*ca*)*b*		*a*(*bc*)*b*	
80 K	100 K	80 K	100 K	80 K	100 K	80 K	100 K
	34 ± 1		37 ± 1	40 ± 2	31 ± 1	40 ± 2	37·5 ± 1
44 ± 1				54 ± 2		57·5 ± 3	
54·5 ± 2		58 ± 3		59 ± 2		68 ± 1	66·5 ± 1
68 ± 1	66 ± 1	68 ± 1	66 ± 1	67·5 ± 1	66 ± 1	98 ± 2	93 ± 3
	92 ± 3		92 ± 3		92·5 ± 2		104 ± 2
100 ± 2	101·5 ± 2	98 ± 3	102 ± 2	100 ± 3	102 ± 3	122 ± 2	120 ± 1
128·5 ± 1	132 ± 1	120·5 ± 2	120 ± 1	121 ± 1	119·5 ± 1	128 ± 2	132 ± 2
152 ± 2	156 ± 3	137 ± 3	133 ± 2	126·5 ± 2		137 ± 2	
168 ± 2	171 ± 2	153 ± 3	150 ± 2	138 ± 3	133·5 ± 3	154 ± 2	
184 ± 3		168 ± 3	172 ± 1	158 ± 3		169 ± 2	175·5 ± 2
195·5 ± 2	200–		176 ± 2	169 ± 2	169·5 ± 2	192 ± 2	
210 ± 3	235	195 ± 2	192 ± 3		174 ± 2	216 ± 2	212 ± 3
218 ± 2		216·5 ± 2	212 ± 3	193 ± 2			296 ± 2
294 ± 3	295 ± 3		295 ± 3	215 ± 3	210·5 ± 3	322·5	
322 ± 2	322 ± 2	322 ± 2			278 ± 3		
					296 ± 2		
				322 ± 2			

† These data are to be read in conjunction with figure 2. Those for MAMC at 295 K are shown in figure 4 and are not readily summarised numerically.

IR spectra were obtained in the range 20–400 cm^{-1} using a Beckman–RIIC FS-720 interferometer with an RS–7F reflectance module. The latter was modified by replacement of the second concave mirror with another of longer focal length as this was found to increase the signal to the detector. A vacuum system capable of giving 5×10^{-5} torr was also installed. Crystals were mounted on a copper plate using an epoxy resin loaded with aluminium powder to increase thermal contact. The plate was attached to the cold station of a CTI-20 closed-cycle cryostat. A Perkin–Elmer polyethylene-based wire grid was used to polarise the light. Spectra were ratioed against those from equivalent runs using a polished copper block in place of the crystal and analysed by the Kramers–Krönig method. Data are in table 3.

The same crystals were used in the same cryostat for the Raman work which was carried out using a Coderg T800 triple monochromator instrument with an EMI 9558B photomultiplier and DC detection. Both MAMC and PAMC showed significant fluorescence at room temperature and this adversely affected the signal/noise ratios. Upon cooling the fluorescence band sharpened and moved to lower energy: the visible effect of this change was that each crystal glowed red when 514·5 nm radiation from the laser was passed through it. Most spectra were measured in both Stokes and anti-Stokes regions to ensure accuracy of the data quoted.

4. Results, assignment and discussion

4.1. Cation modes

A significant feature of the MAMC results is that as the temperature is lowered below ambient the Raman spectra begin to develop a region of broad weak scatter between 250 and 350 cm^{-1}, figure 2. This sharpens to a prominent band at 295 cm^{-1} at 100 K which, on further cooling, weakens rapidly during the change to phase IV and is replaced by a sharper band at 322 cm^{-1}. The PAMC Raman spectra, figure 3 do not show any sharp bands in the interval 250–350 cm^{-1} down to 80 K but are consistent with the behaviour of MAMC in showing a broad region of scatter which increases in prominence as temperature is reduced.

The PAMC Raman spectra of both oriented single crystals and powder samples (at all temperatures used) are distinguished from those of MAMC under equivalent conditions in showing considerable, nearly featureless, scatter as the Rayleigh line is approached. This appears to be consistent with the presence of cation disorder in PAMC at all temperatures down to 80 K. However we cannot rule out the possibility that increased scatter near the Rayleigh line is parasitic, i.e. due to crystal imperfections on a scale comparable with the wavelength of the exciting radiation. In principle these two possible origins could be differentiated by a study of the thermal dependence of the intensity of the scattered light on both Stokes and anti-Stokes sides. In PAMC this is complicated by the presence of temperature-dependent fluorescence which affects the Stokes side especially, and we have not attempted this task in the absence of data-handling facilities. In contrast, a high degree of order in MAMC phases II, III, and IV is suggested by the amount of low-frequency structure in their spectra and the low levels of scatter found below 50 cm^{-1}. However, Peterson and Willett (1972) state that at room temperature PAMC is fully ordered but that there is exceptional thermal motion associated with atoms C_1 and C_2 of the propyl groups: this is tantamount to disorder insofar as the lattice modes are concerned and would seem to account for the Raman observations. PAMC also shows IR features in the 250–300 cm^{-1} region which become more prominent as the temperature is lowered.

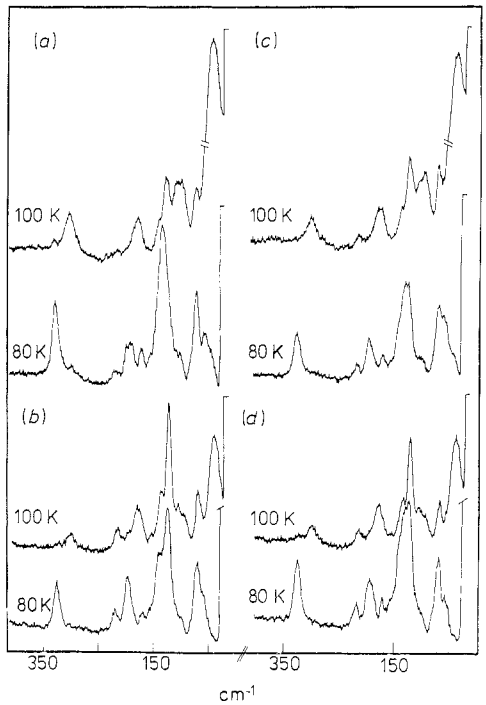

Figure 2. Single-crystal Raman spectra of MAMC phases III and IV. Spectral slit width 3 cm^{-1} (4 cm^{-1}), 75 mW (50 mW) 514·5 nm at the sample at 100 K (80 K). (*a*) *a*(*cc*)*b*, (*b*) *a*(*ca*)*b*, (*c*) *a*(*ba*)*b*, (*d*) *a*(*bc*)*b* where the axes *a*, *b*, *c* are those of orthorhombic phase II.

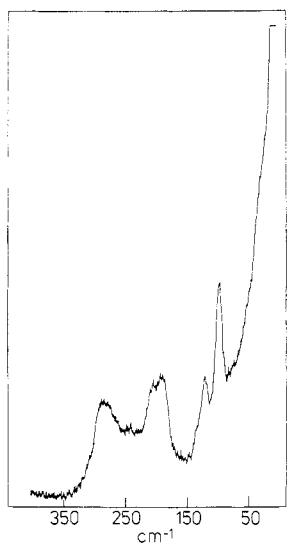

Figure 3. Raman spectra of a randomly oriented crystal of PAMC at 100 K. Spectral slit width 3 cm^{-1} 75 mW 514·5 nm at the sample.

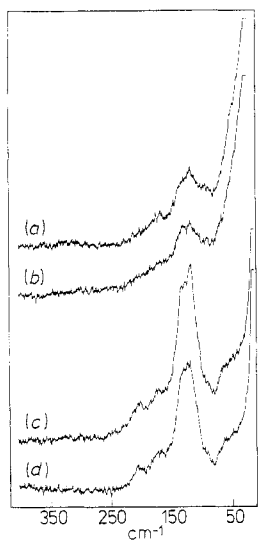

Figure 4. Single-crystal Raman spectra of MAMC phase II at 295 K. Spectral slit width 2·5 cm^{-1}, 75 mW 514·5 nm at the sample. (*a*) *a*(*cc*)*b*, (*b*) *a*(*ca*)*b*, (*c*) *a*(*ba*)*b*, (*d*) *a*(*bc*)*b*.

As argued in § 2, it is most unlikely that any of the anionic sheet modes will be above 260 cm^{-1}. We therefore attribute the features in the 260–350 cm^{-1} interval of MAMC to internal torsions of the cations about their C–N bonds. The cations in PAMC have several internal modes which might also contribute to the 250–350 cm^{-1} region and may help to account for its complexity. They are: torsions about C–C and C–N bonds, and skeletal bends δ(CCC) and δ(CCN).

4.2. Modes below 260 cm^{-1}

Modes below 260 cm^{-1} are all attributed to internal motion of the $[MnCl_4^{2-}]_m$ sheets, together with external modes of the cations which are most probably below 120 cm^{-1}. The gross features of the Raman spectra of randomly oriented crystals of MAMC and PAMC at 100 K concur in showing bands close to 200 cm^{-1}, which we attribute to various forms of ν(Mn–Cl_t) mode, and others in the 90–130 cm^{-1} interval. The cation 'disorder' in PAMC is helpful here in that it is a reasonable presumption that the sharp 98 and 121 cm^{-1} bands originate from the ordered anionic sheet. As shown by table 2(*a*), if the anionic sheets of PAMC had the perfect K_2NiF_4 form the Raman spectra would show only two bands, A_{1g} ν(Mn–Cl_t) stretch and a δ(Mn–Cl_t) bend of E_g type. We consider that the bands in PAMC at about 200 and 100 cm^{-1} respectively are of essentially this origin. We note, especially, that in the K_2NiF_4 type the bridging halogen atoms do not contribute to the *gerade* representation. This implies that in the PAMC case, although the selection rules for the bimolecular-repeat wavy sheet are more complex, the main intensity will still come from δ(Mn–Cl_t) motion.

Comparison of the crystal data for the two materials shows that the Mn–Cl_t bond is a little shorter in PAMC than in MAMC but that the bridge bonds in PAMC are the longer.

Bond length (Å)	MAMC	PAMC
Mn–Cl	2·514	2·475
Mn–Cl_b	2·572	2·629
Δ	0·058	0·154

What is more significant is the difference, Δ, between these two kinds of bond for the two compounds. It implies that there will be a much larger gap between ν(Mn–Cl_t) and ν(Mn–Cl_b) modes in PAMC than in MAMC: the spectra support this. In MAMC there is a fairly continuous series of Raman bands from 250 cm^{-1} downwards whereas in PAMC there is a significant gap at about 130–180 cm^{-1}. The IR reflectance spectra, however, are much more similar.

From these considerations it appears that the main features of the MAMC Raman spectra from about 90 to 140 cm^{-1} are due to deformational modes of the anionic sheets with a major part of the intensity at about 120 cm^{-1} associated with δ(Mn–Cl_t) motion. From about 140 to 250 cm^{-1} there exists a series of bands of which the lowest are principally ν(Mn–Cl_b) and the highest ν(Mn–Cl_t). It is probable that all bands below about 90 cm^{-1} are due to lattice modes, although there must be substantial resonance interaction with sheet internal modes within each symmetry species in so crowded a spectrum. The IR spectra are likely to have a much greater contribution below 200 cm^{-1} from deformational modes associated with the bridging chlorine atoms. In view of the recent demonstration (Stoelinga and Wyder 1976) that two-phonon transitions are significant in infrared spectra of the related layer compounds $[C_nH_{2n+1}NH_3]_2MCl_4$,

($n = 1, 2$; M = Cd, Cu), there can be little doubt that there is a considerable contribution to both IR and Raman spectra from second-order processes in MAMC and PAMC also.

4.3. Raman single-crystal spectra at ambient temperature.

The orthorhombic form of MAMC (phase II) is very close to tetragonal, (a = 7·276, c = 7·215 Å). If it were tetragonal, the following correspondence would exist between our experiments carried out using the standard axis set of *Cmca* (i.e. b normal to the plane of the sheets) and the tetragonal axis set with c normal to the sheets and $a = b$ parallel to orthorhombic a and c respectively.

	D_{2h}^{18}	D_{4h}	D'_{4h}
$a(cc)b$	$A_g(zz)$	$A_g(xx)$	$A_g(x'x')$
$a(ba)b$	$B_{1g}(yx)$	$E_g(xz)$	$E_g(x'z + y'z)$
$a(ca)b$	$B_{2g}(zx)$	$B_{2g}(xy)$	$B_{1g}(x'x')$
$a(bc)b$	$B_{3g}(yz)$	$E_g(zy)$	$E_g(x'z + y'z)$

The close correspondence between our *ba* and *bc* spectra, figures 4 and 2, indicates that the departure from tetragonal is too slight to affect the Raman spectra significantly. We also find that the *cc* and *ca* spectra are closely similar. This is readily accounted for if the pseudo-tetragonal axis set is taken with c defined as above, but with $a = b$ axes at 45° to the orthorhombic a-, c-axes. The effect (column D'_{4h}) is to cause both $a(cc)b$ and $a(ca)b$ experiments to yield what in D'_{4h} are $A_g + B_{1g}$ species.

Although the spectral behaviour of this phase is pseudo-tetragonal insofar as the oriented spectra are concerned it has much more complex spectra than can be accounted for on the basis of the K_2NiF_4 structure, table 2(*b*). In fact the spectra near ambient temperature consist of such broad regions of scattering that no unambiguous count can be made of the numbers of bands contributing to the spectra. Theory allows the Raman spectra to show up to 24 bands, that is, the sum of rows N_s, T, and R of table 2(*a*). However, the pseudo-tetragonal behaviour shows that the 11 $A_g + B_{2g}$ modes must lie within the envelope shown in figure 4(*a*) and that the 13 $B_{1g} + B_{3g}$ modes are similarly within the envelope of figure 4(*c*). Since lowering the temperature to decrease half bandwidths precipitates a phase transition there would appear to be no way in which further detail can be extracted from these spectra, which are more like density-of-states functions than spectra, using simple Raman technique. However, a valuable distinction between sheet internal modes and cation external modes could most probably be made using resonance Raman spectroscopy. Resonance within the $[MnCl_4^{2-}]$ chromophore should reveal which bands are due to modes originating there. We note that, if we are correct in believing that the region 100–250 cm^{-1} is solely due to modes of the $[MnCl_4^{2-}]_m$ sheets, the spectra of figures 4(*a*) and 4(*c*) should show five ($A_g + B_{2g}$) and seven ($B_{1g} + B_{3g}$) bands respectively in that region; in view of the appearance of the spectra credibility is not strained by this suggestion. Analogous remarks apply to PAMC.

4.4. IR *reflectance spectra at ambient temperature*

The 295 K spectra of orthorhombic MAMC in both polarisations with the electric vector normal to the sheet stacking direction show three regions of reflection. There is some indication in the experimental reflectance spectra of structure on each main band but we have been conservative in the ϵ'' maxima we have listed, although there are further

shoulders on the ϵ'' functions. The spectra in the two $\boldsymbol{E} \perp b$ polarisations are effectively identical, again indicating pseudo-tetragonal behaviour. Of the three main bands, that at 225 cm^{-1} must be associated principally with ν(Mn–Cl) motion. The selection rules for the parent K_2NiF_4 structure, table 2(*b*), show that if the sheet were perfectly tetragonal there would be four E_u modes, one of which is a cation translatory mode. The other three E_u modes involve internal coordinate sets which describe respectively: (i) a $\nu(Mn–Cl_b)$ mode of the $Mn–Cl_b$ bonds in the plane of the sheet; (ii) $\delta(Mn–Cl_b)$ of the same planar part of the sheet; (iii) $\delta(Mn–Cl_t)$ in which the $Mn–Cl_t$ bonds normal to each sheet are deformed. In SnF_4 (Beattie *et al* 1971) the two E_u deformations are at 245, 265 cm^{-1}, and the $\nu(Sn–F_b)$ mode at 472 cm^{-1}. Accordingly we attribute the broad intense region at about 130 cm^{-1} in MAMC to a near-coincident pair of E_u deformation modes of the sheet, some of the breadth of the band deriving from Fermi resonance interaction between them, rather than from a large damping constant associated with a single band. In support of this view we note that at low temperatures considerably more structure is developed in this region than in the 230 ± 30 cm^{-1} interval which is believed to contain a single E_u mode.

By elimination the 110 cm^{-1} band is attributed to the sole E_u cation translatory mode, which is in the right sort of region. $CH_3NH_3^+$ and K^+ have similar masses and the same charge: their translatory modes are to be expected at similar frequencies. In a considerable number of K^+ salts of chloroanionic species these modes come at 100 ± 20 cm^{-1} (Adams 1967).

In terms of the FGA the two orientations should show $8B_{1u}$ ($\boldsymbol{E} \| c$) and $6B_{3u}$ ($\boldsymbol{E} \| a$) bands. As with the Raman spectra, the breadths of the bands are such that they show less than the predicted detail, although they could certainly encompass these numbers of contributions as well as second-order features.

The IR reflectance spectra of PAMC, obtained by analogous experiments, are plainly different from other each (figures 5(*a*) and (*b*)) and do not suggest pseudo-tetragonal

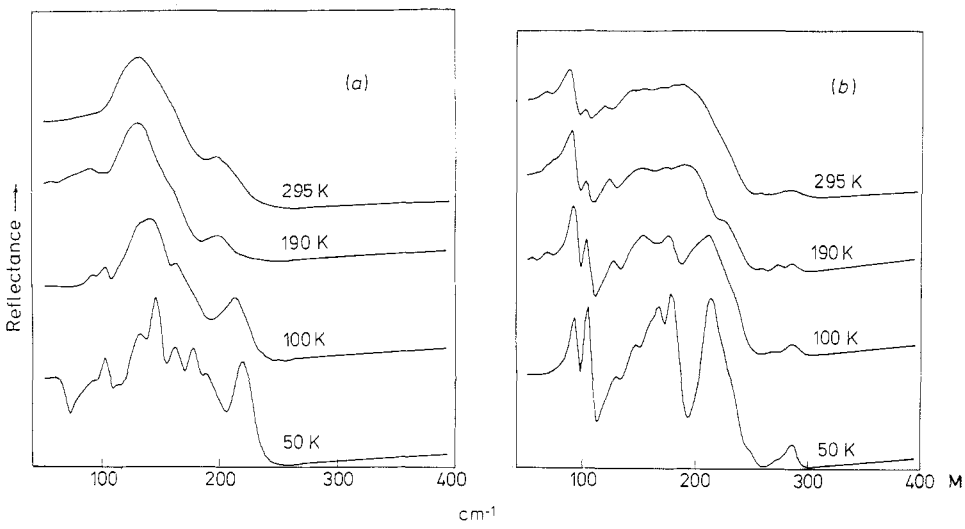

Figure 5. Far-IR reflectance spectra of PAMC at various temperatures. (*a*) $\boldsymbol{E} \| c$, (*b*) $\boldsymbol{E} \| a$.

behaviour. This reflects the much greater difference between the two axes normal to the sheet stacking direction ($\Delta = 0{\cdot}22$ Å; cf. 0·06 Å for MAMC). The $\boldsymbol{E} \| c$ spectra show less than the predicted numbers of bands but for $\boldsymbol{E} \| a$ at least six of the predicted $8B_{1u}$ modes were observed up to 260 cm^{-1}, and there is certainly an unresolved shoulder on the ϵ'' curve, figure 6, at about 160 cm^{-1} making seven modes in all. We consider that the 68 and 85 cm^{-1} bands (295 K) are due to the two cation translatory modes (table 2*a*) with, possibly, a contribution from the sole rotatory mode. Since the $Mn–Cl_t$ bond length in PAMC is short compared with that in MAMC we suggest that the 257 cm^{-1} band is the expected B_{1u} $\nu(Mn–Cl_t)$ mode; the unresolved component at about 160 cm^{-1} is then assigned to the single $\nu(Mn–Cl_b)$ mode allowed in this species (B_{1u}).

4.5. The IR *and Raman spectra of phases III and IV of* MAMC

Phase III of MAMC is known to be tetragonal. In accord with this we find that the IR reflectance spectra (obtained at 100 and at 190 K) are identical for the two orientations of the electric vector normal to the sheet stacking axis, figures 7 and 8. These spectra show more features than those of phase II, although they are evidently similar in their overall shape. The additional bands can be accommodated on the basis outlined in the

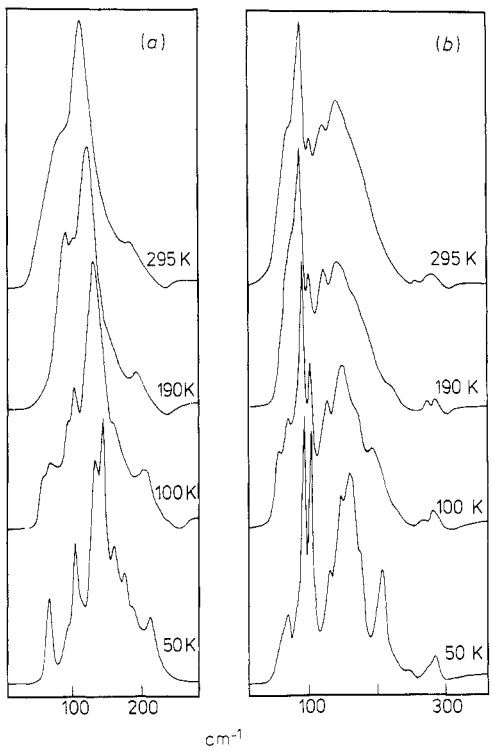

Figure 6. The imaginary part, ϵ'', of the dielectric constant for PAMC at various temperatures. (*a*) $\boldsymbol{E} \| c$. (*b*) $\boldsymbol{E} \| a$.

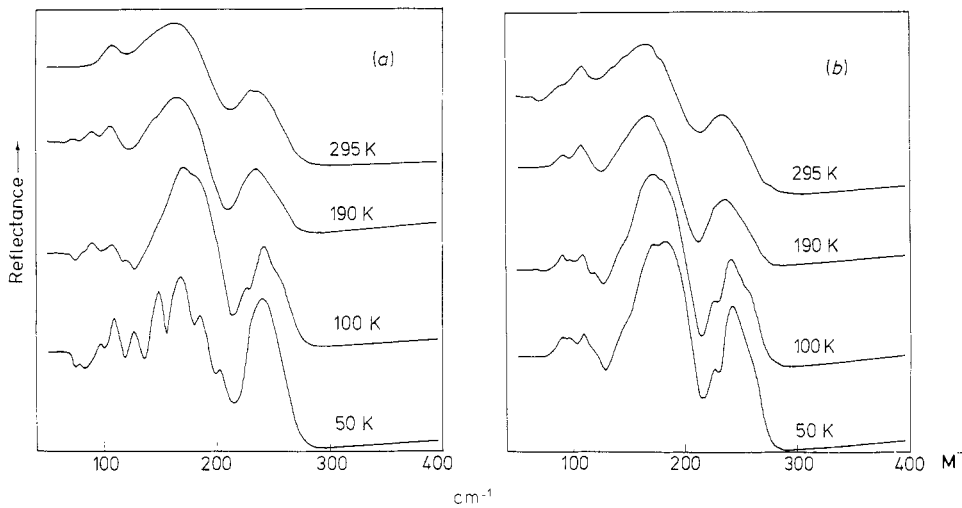

Figure 7. Far-IR reflectance spectra of MAMC at various temperatures, (*a*) $\boldsymbol{E} \| c$ (*b*) $\boldsymbol{E} \| a$.

remarks on selection rules which included the suggestion that doubling of the primitive cell (from that of phase II) takes place.

The transition to the monoclinic phase IV is heralded by appearance at 50 K of very different spectra from the same two orientations of the electric vector. These substantially different spectra imply that the electric vector remains parallel to two of the indicatrix

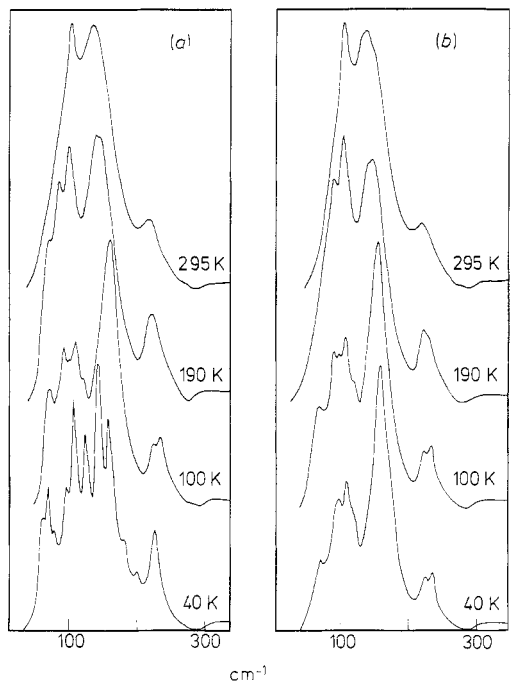

Figure 8. The imaginary part, ϵ'', of the dielectric constant for MAMC at various temperatures. (a) $E \| c$, (b) $E \| a$.

axes of the new phase. This view is supported by the result of a reflectance experiment in unpolarised radiation which yielded a much more complex spectrum than those with polarised light and which was identical with the 70 K spectrum shown by Lehner *et al* (1975) for $\boldsymbol{E} \perp c$ (i.e. equivalent to our $\boldsymbol{E} \perp b$). This complex spectrum was clearly seen to be the sum of our $\boldsymbol{E} \parallel a$ and $\boldsymbol{E} \parallel c$ spectra.

It is unlikely that this new complexity shown by phase IV arises from further multiplication of the primitive cell content since a monoclinic cell is not often greater than tetramolecular. More probably it is due to the lifting of degeneracies and the relaxation of selection rules which caused some modes to be inactive in phase III.

Raman spectra of phase III are broadly in agreement with the expectations for a tetragonal phase; the (*ba*) and (*bc*) spectra remain similar, as do the (*cc*) and (*ca*) pair. However, phase IV yielded spectra which, in all orientations, are rather similar in appearance, but significantly changed from those of phase III. It is probable that the similarities shown by these phase IV Raman spectra are due as much to polarisation scrambling caused by development of polycrystallinity as to inherent mode structure. The most important difference is in the region below 80 cm^{-1}; an intense broad band at about 35 cm^{-1} in III is lost and its taken to represent the modes most involved in driving the structural transition to phase IV. Concurrently a group of bands at about 90–105 cm^{-1} appears to move upwards some 25 cm^{-1} causing an intensity increase of about 115–140 cm^{-1}. Since these changes are accompanied by the events at about 300 cm^{-1} attributed above to the onset of well-defined cation internal torsions, we consider that the lower-frequency regions indicated are chiefly due to external motions of the same cations. This conclusion is strengthened by comparison with equivalent spectra for PAMC which, having different cations, shows quite different behaviour below 100 cm^{-1}. That this freezing of the MAMC lattice affects the wavy sheet is only to be expected and is reflected in the changes of detail in the 150–220 cm^{-1} where there is a high density of states of deformational modes.

4.6. The low-temperature behaviour of PAMC

The phase transition temperatures have not yet been established for this material. However, the IR-reflectance spectra are consistent with transitions to new phases at temperatures similar to those of MAMC. The differences between spectra with $\boldsymbol{E}$ parallel to *a* and to *c*, noted at ambient temperature, persist implying that phase III is orthorhombic rather than tetragonal. There can be little doubt that phase IV is monoclinic in view of its spectral complexity.

Raman spectra of this material, even at 80 K, were less well-defined than for MAMC. The prominent band at 99 cm^{-1} is taken to correspond to the one at 120 cm^{-1} in MAMC and to be correlated with anion sheet deformational modes because it is known that the Mn–Cl_b bonds are longer in PAMC.

5. Conclusions

For reasons discussed in the text the usual single-crystal methods do not work well when applied to the phases II stable near ambient temperature. The data for lower-temperature phases are much more precise but must await more complete crystallographic information before they can be adequately interpreted. Nevertheless, the principal features of all the spectra are a broad central region at about 100–200 cm^{-1}

containing the many deformational modes of the wavy anion sheets bounded to higher frequency by ν(Mn–Cl) modes and tailing off below 150 cm^{-1} into a series of structure-sensitive cation external motions. Further work is required using crystals containing deuteriated cations, and the resonance Raman suggestion (above) should be followed up, so that more complete understanding of the phonon spectra of these crystals may be achieved.

Acknowledgment

We thank the SRC for a grant (to DCS).

References

Adams D M 1967 *Metal–Ligand and Related Vibrations* (London: Arnold)
Adams D M and Newton D C 1970 *Tables for Factor Group and Point Group Analysis* (Croydon: Beckman-RIIC)
—— *J. Chem. Soc.* A**00** 3499
Adams D M and Smardzewski R R 1971 *Inorg. Chem.* **10** 1127
Arend H, Hofmann R and Waldner F 1973 *Solid St. Commun.* **13** 1629
Beattie I R, Cheetham N, Gilson T R, Livingstone K M S and Reynolds D J 1971 *J. Chem. Soc.* A**00** 1910
Blinc R, Burgar M, Lozar B, Seliver J, Slak J, Rutar V, Arend H and Kind R 1977 *J. Chem. Phys.* **66** 278
Bocanegra E H, Tello M J, Arrandiaga M A and Arend H 1975 *Solid St. Commun.* **17** 1221
Brinkmann D, Walther U and Arend H 1976 *Solid St. Commun.* **18** 1307
Chapuis G, Arend H and Kind R 1975 *Phys. Stat. Solidi* A **31** 455
Chapuis G, Kind R and Arend H 1976 *Phys. Stat. Solidi* A **36** 285
Edwards H G M, Ware M J and Woodward L A 1968 *Chem. Commun.* **00** 540
Heger G, Henrich E and Kanellakopulos B 1973 *Solid St. Commun.* **12** 1165
Heger G, Mullen D and Knorr K 1975 *Phys. Stat. Solidi* A **31** 455
—— 1976 *Phys. Stat. Solidi* A **35** 627
Kind R and Roos J 1976 *Phys. Rev.* B **13** 45
Knorr K, Jahn I R and Heger G 1974 *Solid St. Commun.* **15** 231
Lehmann W and Weber R 1973 *Phys. Lett.* **45**A 33
Lehner N, Strobel K, Geick R and Heger G 1975 *J. Phys. C: Solid St. Phys.* **8** 4096
Levstik A, Filipic C, Blinc R, Arend H and Kind R 1976 *Solid St. Commun.* **20** 127
Peterson E R and Willett R D 1972 *J. Chem. Phys.* **56** 1879
Seliger J, Blinc R, Kind R and Arend H 1976 *Z. Phys.* **25**B 189
Stoelinga J H M and Wyder P 1976 *J. Chem. Phys.* **64** 4612